Eksakta : Berkala Ilmiah Bidang MIPA
VOLUME 27 NO 03 2026, pp 361-373
ISSN : Print 1411-3724 — Online 2549-7464
DOI : https://doi.org/10.24036/eksakta/vol27-iss03/701

Eksakta
Berkala Ilmiah Bidang MIPA
http://www.eksakta.ppj.unp.ac.id/index.php/eksakta

Article

Analysis of Fault Plane and Distribution of Coulomb Stress Changes of the M_w 7.8 Earthquake Southwest of Sumatra

Article Info

Article history :
Received May 26, 2026
Revised June 10, 2026
Accepted June 16, 2026
Published June 30, 2026

Keywords :
Coulomb stress change,
aftershock
finite fault
nodal plane

Gabriela[1], Kelly Lasofia Br Girsang[1], Rizki Wulandari[1,2*] Yudha Styawan[1,2]

[1]Department of Geophysical Engineering, Faculty of Industrial Technology, Institut Teknologi Sumatera, Lampung, Indonesia
[2]Center for Earthquake and Tsunami Disaster Mitigation, Institut Teknologi Sumatera, Indonesia

Abstract. Precise identification of the true fault plane and accurate quantification of Coulomb stress redistribution are fundamental prerequisites for seismic hazard assessment in intraplate deformation zones. However, the complexity of the conjugate fault system in the Wharton Basin characterized by the reactivation of ancient oceanic crust along north–south and northwest–southeast orientations, introduces significant ambiguity in nodal plane discrimination, leaving the rupture mechanism and post-seismic stress transfer patterns in this region poorly constrained. Given that this zone has demonstrated persistent seismicity capable of threatening the southwestern Sumatran region, accurate seismic hazard evaluation is critically urgent. This study aims to identify the true fault plane, characterize the spatial distribution of Coulomb stress change ($\Delta\sigma_c$), and evaluate the spatial consistency between positive stress zones and aftershock distribution as a proxy for stress model validation, using the Coulomb stress change ($\Delta\sigma_c$) method based on focal mechanism parameters and finite fault models obtained from the USGS. Results indicate that Nodal Plane 1 represents the true fault plane, exhibiting maximum stress increases of up to 0.1 bar-oriented west–east to northwest–southeast, consistent with the active tectonic structure of the Wharton Basin. Evaluation of aftershocks reveals higher spatial consistency with positive $\Delta\sigma_c$ zones on Nodal Plane 2 as the receiver fault, whereas the relative inconsistency on Nodal Plane 1 suggests that oceanic crustal heterogeneity and intraplate rupture complexity jointly govern post-seismic seismicity distribution beyond the contribution of static stress transfer alone.

Corresponding Author :
Rizki Wulandari
Department of Geophysical Engineering, Faculty of Industrial Technology,
Institut Teknologi Sumatera, Lampung, Indonesia
Email : rizki.wulandari@tg.itera.ac.id

1. Introduction

The Wharton Basin, situated in the northeastern Indian Ocean southwest of Sumatra, constitutes one of the most seismically active intraplate deformation zones in the world. This basin is underlain by ancient Eocene-era oceanic crust intersected by a dense network of fossil fracture zones, extinct spreading ridges, and reactivated transform faults predominantly oriented north–south and northwest–southeast, as illustrated in the regional tectonic framework of the Wharton Basin and its surrounding regions (Figure 1) [1-2].

These inherited structural weaknesses are particularly susceptible to reactivation under the contemporary compressional and transpressional stress regime driven by the ongoing convergence between the Indo-Australian and Eurasian plates [2]. Unlike seismicity at plate boundaries, earthquakes within the Wharton Basin nucleate on reactivated ancient oceanic faults far from any well-defined plate margin, producing complex intraplate rupture patterns that are inherently difficult to characterize using conventional seismotectonic frameworks [3]. The conjugate geometry of these fracture zones, accommodating both left-lateral strike-slip motion along north–south trending structures and right-lateral motion along oblique shear zones, creates a highly heterogeneous stress environment that complicates fault plane identification from focal mechanism data alone [4-5].

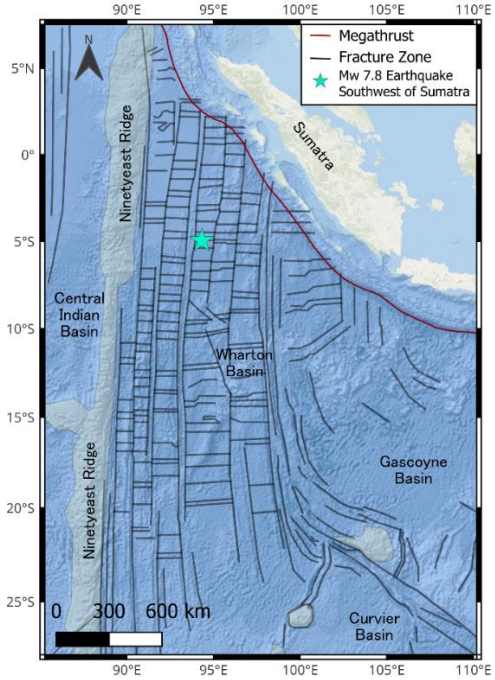

Figure 1. Fracture zones Wharton Basin Black lines indicate fracture zones, red lines show the megathrust, and green star marks the location of the M_w 7.8 earthquake southwest of Sumatra. Modified from Jacob et al., 2014.

The seismic significance of the Wharton Basin became globally prominent following the 2004 M_w 9.2 Sumatra-Andaman megathrust earthquake, which transferred substantial Coulomb stress into the intraplate domain and triggered the subsequent 2012 M_w 8.6 and M_w 8.2 strike-slip sequence, the

largest intraplate earthquakes ever instrumentally recorded. The 2004 rupture promoted widespread seismicity across the Wharton Basin, with at least one nodal plane of 95% of subsequent $M_w \geq 4$ events experiencing positive stress loading, and that the regional stress field likely governed the sub-fault orientations of the 2012 M_w 8.6 mainshock [6]. Extending this seismic sequence, an M_w 7.8 strike-slip earthquake occurred on March 2, 2016, located at 4.952°S and 94.330°E at a depth of 24 km in the southern Wharton Basin. The USGS finite fault model indicates heterogeneous coseismic slip concentrated on a north–south trending rupture plane, consistent with the reactivation of a fossil transform fault within the ancient oceanic lithosphere [7]. This event represents a significant continuation of intraplate seismic activity and constitutes an important case study for investigating fault reactivation mechanics and Coulomb stress redistribution in the Wharton Basin.

Coulomb stress change ($\Delta\sigma_c$) analysis provides a well-established quantitative framework for evaluating coseismic stress redistribution by combining shear stress change ($\Delta\tau$) and normal stress change ($\Delta\sigma_n$) resolved onto specified fault planes [8]. Positive $\Delta\sigma_c$ values indicate increased failure potential and are widely associated with elevated aftershock probability, whereas negative values denote stress shadow zones characterized by suppressed seismic activity [9]. This approach has been extensively applied along the Sumatra-Andaman subduction system; however, its systematic application to purely intraplate rupture environments within the Wharton Basin, particularly for events post-dating the 2012 sequence, remains comparatively limited [8]. Sukrungsri et al. (2024) examined co-seismic stress changes for six $M_w \geq 7$ earthquakes along the Sumatra–Andaman arc, demonstrating that spatial consistency between positive $\Delta\sigma_c$ zones and observed aftershocks are strongly sensitive to receiver fault geometry and focal mechanism type [10]. Tian et al. (2022) identified 12 large active faults trending NWW–SEE in the northern Wharton Basin, yet their specific role in controlling post-seismic stress transfer from the 2016 M_w 7.8 rupture has not been quantitatively evaluated [8].

Despite these advances, no study has yet conducted a dedicated $\Delta\sigma_c$ analysis of the 2016 M_w 7.8 Wharton Basin earthquake as an independent intraplate event, with explicit nodal plane discrimination and spatial validation against observed aftershock distribution. Although Guo et al. (2021) established the regional Coulomb stress framework following the 2004 and 2012 events, their analysis did not extend to the 2016 rupture, which reactivated a distinct north–south trending fossil transform fault at approximately 5°S-geometrically different from the WNW–ESE sub-faults dominant in the 2012 sequence [6]. Previous Coulomb studies in Sumatra focused predominantly on subduction zone and Sumatran Fault Zone contexts, and therefore did not address the nodal plane ambiguity inherent to the conjugate fault system of the southern Wharton Basin [11-12]. Furthermore, no prior study has quantitatively assessed the degree to which the $\Delta\sigma_c$ model for the 2016 event explains the spatial distribution of its associated aftershocks, which is a critical validation step for confirming the true fault plane identity. Addressing this gap is particularly urgent given the sustained elevated seismicity in the southern Wharton Basin since the 2012 sequence and the need for accurate stress hazard characterization in the southwestern Sumatran region.

This study aims to address the aforementioned gap through systematic $\Delta\sigma_c$ analysis of the 2016 M_w 7.8 Southwest Sumatra earthquake using focal mechanism parameters and the USGS finite fault model. The first objective is to identify the true fault plane by comparing $\Delta\sigma_c$ patterns generated by Nodal Plane 1 (NP1: strike 274°, dip 84°, rake 169°) and Nodal Plane 2 (NP2: strike 5°, dip 79°, rake 6°) against the regional tectonic structure of the Wharton Basin. The second objective is to characterize the spatial distribution of Coulomb stress changes on both nodal planes and assess their orientational consistency with active structures in the southern Wharton Basin. The third objective is to evaluate the spatial consistency between positive $\Delta\sigma_c$ zones and the distribution of aftershocks as a quantitative proxy for stress model validation. These findings are expected to advance understanding of intraplate fault reactivation and stress transfer dynamics in the Wharton Basin, contributing to improved seismic hazard assessment in the southwestern Sumatran region.

2. Research Methodology

2.1. Materials

This study employs the static Coulomb stress change ($\Delta\sigma_c$) approach to quantify stress redistribution induced by the 2016 M_w 7.8 Southwest Sumatra earthquake. The Coulomb stress change ($\Delta\sigma_c$) is calculated using the following expression:

$$\Delta\sigma_c = \Delta\tau + \mu'\Delta\sigma_n \qquad (1)$$

where $\Delta\tau$ represents shear stress change in the slip direction, $\Delta\sigma_n$ is the normal stress change (positive for compression), and μ' is the effective friction coefficient, which measures the frictional resistance at the fracture plane by accounting for the effect of pore fluid pressure [13]. An effective friction coefficient μ' of 0.40 was adopted in the Coulomb stress calculations. This value has been widely used in previous Coulomb stress transfer studies because it represents typical frictional conditions on crustal faults and provides reasonable estimates of stress interactions following large earthquakes [14]. Positive ($\Delta\sigma_c$) values indicate increased fault instability, while negative values indicate stabilization. In the context of seismic geophysics, this analysis is a key component in reconstructing source processes, understanding interactions between fault segments, and assessing seismic hazard based on stress changes [15].

The data used in this study consists of the epicenter data for the earthquake that occurred in southwest Sumatra on March 2, 2016. The data used, which includes the parameters of the main earthquake, can be seen in Table 1, as well as the slip distribution data (finite fault) from the USGS last accessed in June 2026 [7]. Furthermore, aftershock events with magnitudes $M_w \geq 4$ occurring within one month after the mainshock (March 2, 2016–March 31, 2016) were retrieved from the USGS earthquake catalog and are presented in Table 2. Data on previous major earthquakes were obtained from the Global Centroid Moment Tensor Catalog (GCMT) last accessed in June 2026 [16].

Table 1. Parameters of mainshock (USGS, 2026)

Time	Long (°)	Lat (°)	*Depth* (km)	Location
2016-03-02	94.330	-4.952	24	*Southwest of Sumatra*, Indonesia

Table 2. Parameters of aftershock (USGS, 2026)

Time	Long (°)	Lat (°)	*Depth* (km)	Magnitude
2016-03-10	94.4541	-4.6746	10	4.4
2016-03-05	94.5165	-4.6495	10	4.5
2016-03-04	94.4205	-4.1881	10	5.4
2016-03-04	94.4876	-4.9749	10	4.7
2016-03-03	94.5248	-4.6865	15.23	4.4
2016-03-03	94.5657	-4.8577	10	4.7
2016-03-03	94.3177	-4.5172	10	4.5
2016-03-03	94.3595	-4.5413	10	4.8
2016-03-03	94.1623	-4.519	10	4.5
2016-03-03	94.2857	-4.6505	17.55	4.5
2016-03-03	94.2839	-4.5235	10	4.3
2016-03-03	94.4101	-4.794	10	5.6
2016-03-02	94.3203	-4.496	15.69	4.4
2016-03-02	94.007	-4.9812	14.31	4.3
2016-03-02	94.2744	-4.8224	12.33	5.1
2016-03-02	94.3243	-4.6945	10	4.6

Table 3. Fault parameters (USGS, 2026)

Plane	Strike	Dip	Rake	Focal Mechanism
Nodal Plane 1	274°	84°	169°	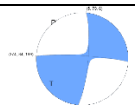
Nodal Plane 2	5°	79°	6°	

2.2. Modeling Procedure

The primary method used in this study is the Coulomb Stress Change analysis, which was calculated using the Coulomb 3.4 software. This method is widely applied to examine the distribution of shear stress (τ) and normal stress ($\Delta\sigma$) in rocks in response to earthquakes [17]. The initial phase of the study involved collecting earthquake source data, including parameters for the mainshock and aftershocks from the USGS catalog [7], as well as fault parameters in the form of moment tensor data from the Global CMT [16]. Aftershocks were selected within approximately one month following the main event to represent the initial post-earthquake seismicity response [18].

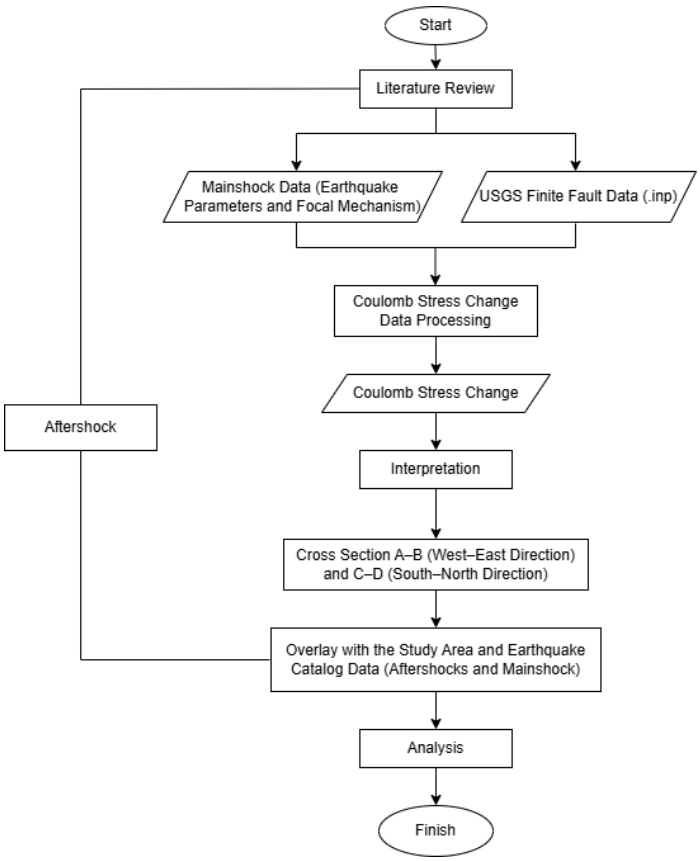

Figure 2. Research Workflow

Subsequently, a seismicity map was created to display the distribution of the main earthquake and aftershocks using QGIS software, which served as the basis for visualizing stress changes in the study area.

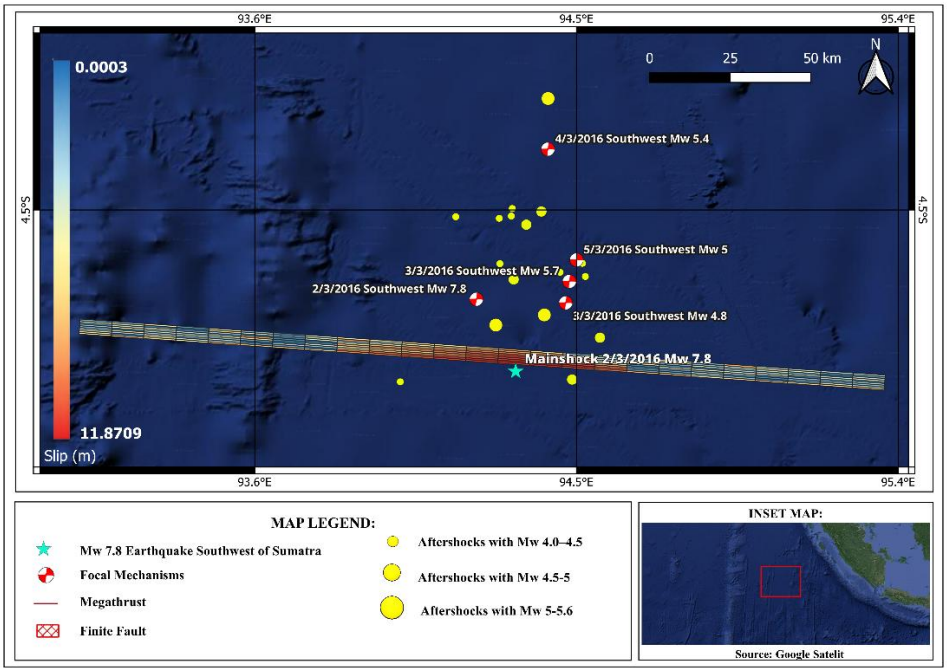

Figure 3. Seismicity map and finite-fault model of the 2016 Southwest Sumatra earthquake. The red line represents the megathrust zone, while the green star indicates the M_w 7.8 mainshock that occurred southwest of Sumatra. The focal mechanisms illustrate the faulting characteristics of earthquakes surrounding the mainshock area. Yellow circles denote aftershock events, where symbol size corresponds to earthquake magnitude: small circles represent M_w 4.0-4.5, medium circles represent M_w 4.5-5.0, and large circles represent M_w 5.0-5.6. The finite-fault model describes the spatial distribution of coseismic rupture associated with the mainshock.

Seismicity is a representation of earthquake activity based on location and time, showing how the Earth's crust responds to the accumulation and release of tectonic stress [19]. Figure 2 shows the seismicity map and finite fault map of Southwest Sumatra, which are important for understanding earthquake distribution patterns, source characteristics, and their relationship with geological structures and regional stress conditions. In the next step, the parameters of Nodal Plane 1 and Nodal Plane 2 were extracted from the moment tensor data of major earthquakes and then processed separately to identify the true fault plane and the auxiliary nodal plane, thereby allowing for a comprehensive analysis of both possible orientations of the source mechanism [20].

Each nodal plane is used as the basis for calculating static stress changes to obtain the distribution of shear stress ($\Delta\tau$), normal stress ($\Delta\sigma_n$) , and Coulomb stress change ($\Delta\sigma_c$) according to the orientation of the analyzed fault [21]. Slip parameters and fault geometry are obtained from the USGS finite fault model, as shown in Figure 3, which was constructed through the inversion of global seismic wave data, co-seismic GPS, and teleseismic body waves to generate realistic slip distributions along the fault plane. This approach allows for an evaluation of the influence of variations in fault plane orientation on stress change patterns and their implications for the potential for post-earthquake seismic activity [22].

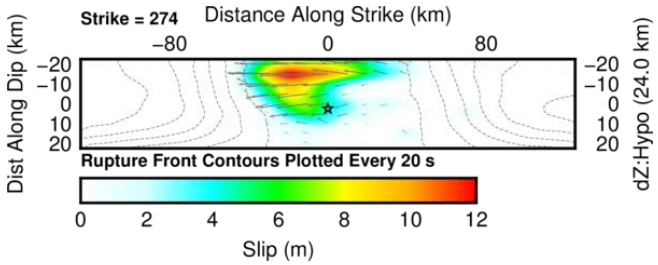

Figure 4. Location of the M_w 7.8 earthquake off the southwest coast of Sumatra in 2016 (USGS, 2025)

3. Results and Discussion

The M_w 7.8 earthquake in Southwest Sumatra on March 2, 2016 produced two nodal planes, each generating a distinct Coulomb stress distribution pattern. Identifying the true fault plane requires selecting the nodal plane whose geometry is most consistent with the finite fault model, regional tectonic structure, and aftershock distribution [23]. The USGS finite fault model (Figure 3) explicitly adopts a strike of 274°, which corresponds directly to the orientation of Nodal Plane 1 (NP1: strike 274°, dip 84°, rake 169°), confirming that Nodal Plane 1 (NP1) is the geometry selected for official rupture modeling [7]. The geological framework of the Wharton Basin, traversed by fossil fracture zones and ancient transform faults predominantly oriented west-east to northwest-southeast, further supports Nodal Plane 1 (NP1) as the structurally coherent rupture plane [24]. Based on this consistency, NP1 is identified as the primary candidate for the true fault plane controlling the source mechanism of this earthquake.

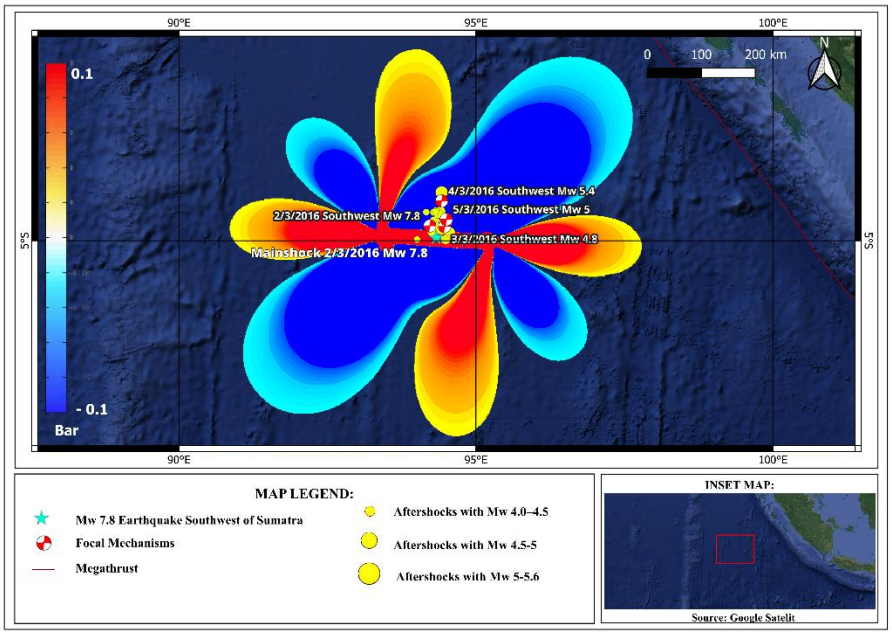

Figure 5. Coulomb stress change map of the 2016 Southwest Sumatra earthquake based on Nodal Plane 1. The map shows the spatial distribution of Coulomb stress variations, where blue regions indicate a decrease in Coulomb stress, while red regions indicate an increase in Coulomb stress following the mainshock event. The red line represents the megathrust zone, and the green star marks the M_w 7.8 Southwest of Sumatra earthquake. Focal mechanisms illustrate the faulting characteristics of surrounding earthquakes, and yellow circles represent aftershock events distributed around the mainshock area.

Distribution of Coulomb stress changes generated by the M_w 7.8 earthquake in southwest Sumatra on March 2, 2016, along with the focal mechanism solution and the spatial distribution of aftershocks in the surrounding area (Figure 5). Warm colors (yellow to red) indicate positive Coulomb stress changes that promote fault rupture, while cool colors (blue) represent negative stress changes that inhibit fault rupture. The circles indicate aftershocks with magnitudes >4, and the red line indicates the megathrust zone off the west coast of Sumatra. The focal mechanism ("beach ball") represents the fault geometry of the main earthquake used in the stress transfer analysis [25]. When Nodal Plane 1 is used as the source plane, the distribution of Coulomb stress changes ($\Delta\sigma_c$) shows a significant increase in stress from 0 to 0.1 bar.

Table 4. Percentage distribution of aftershocks in the stress-increase and stress-decrease zones on Nodal Plane 1 (NP1) and Nodal Plane 2 (NP2)

Plane	($\Delta\sigma_c > 0$)	Percentage (%)	($\Delta\sigma_c < 0$)	Percentage (%)
Nodal Plane 1	4	28.57	10	71.43
Nodal Plane 2	10	71.43	4	28.57

Although NP1 is identified as the true fault plane, a spatial anomaly is observed approximately 71.43% of the recorded aftershocks ($M_w \geq 4.0$) are located within the negative $\Delta\sigma_c$ zones of Nodal Plane (NP1) (Table 4). This anomaly is primarily explained by the exceptionally high coseismic stress drop of ~200 bar which creates an unusually broad stress shadow that geometrically encompasses most aftershock locations proximal to the compact rupture zone [26]. Hardebeck and Harris (2022) demonstrated that aftershock rates in static stress shadow zones do not fall below background seismicity rates, and that such aftershocks are most consistent with dynamic stress triggered by near-field seismic waves rather than static Coulomb stress transfer [27]. Furthermore, uncertainties inherent in ($\Delta\sigma_c$) calculations particularly those arising from variations in receiver fault geometry, friction coefficient, and strike orientation of the receiver plane, may produce localized positive stress concentrations within the broader modeled stress shadow that are not fully resolved by the simplified elastic half-space model [28]. Additionally, the spatially heterogeneous pre-stress state of the 40-80 Ma oceanic crust generates localized positive stress concentrations within the broader modeled stress shadow that are not resolved by the simplified elastic half-space model [29].

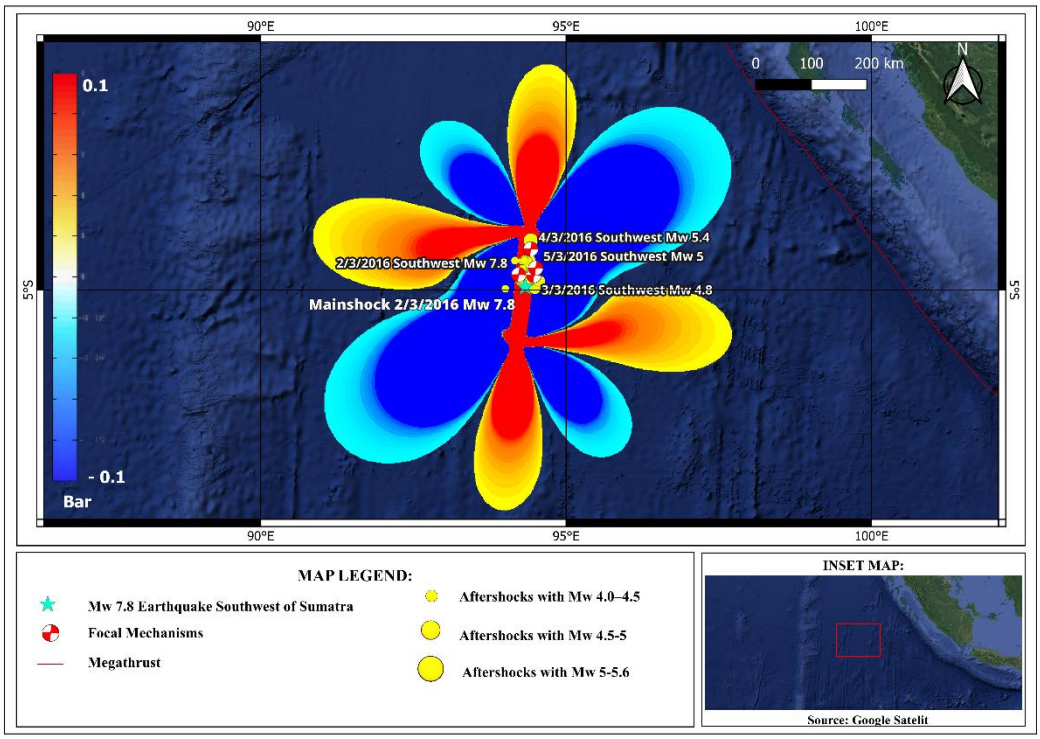

Figure 6. Coulomb stress change map of the 2016 Southwest Sumatra earthquake based on Nodal Plane 2. The map shows the spatial distribution of Coulomb stress variations, where blue regions indicate a decrease in Coulomb stress, while red regions indicate an increase in Coulomb stress following the mainshock event. The red line represents the megathrust zone, and the green star marks the M_w 7.8 Southwest of Sumatra earthquake. Focal mechanisms illustrate the faulting characteristics of surrounding earthquakes, while yellow circles represent aftershock events distributed around the mainshock area.

Nodal Plane 2 (strike 5°, dip 79°, rake 6°) exhibits a north-south to west-east orientation that is less consistent with the dominant tectonic fabric of the Wharton Basin (Figure 5). Although the positive $\Delta\sigma_c$ zones of Nodal Plane 2 show higher spatial consistency with the observed aftershock distribution, this result reflects static stress transfer from the Nodal Plane 1 rupture onto conjugate north-south trending fossil fracture zones rather than rupture along Nodal Plane 2 itself.

Guo et al. (2021) demonstrated that the regional maximum compressive stress in the Wharton Basin is oriented at 153 plus or minus 18 degrees, which is more consistent with the Nodal Plane orientation than with Nodal Plane 2, confirming that Nodal Plane 1 is better aligned with the regional stress field driving fault reactivation [6]. Therefore, Nodal Plane 2 is interpreted as an accommodates post-seismic stress transfer from the Nodal Plane 1 mainshock rupture, rather than as the primary rupture plane [15][30]. The stress increase on Nodal Plane 2 indicates that north-south trending secondary structures in the vicinity carry elevated failure potential following the 2016 mainshock.

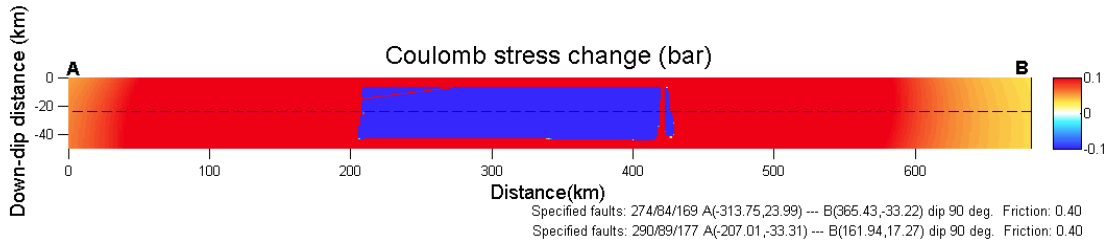

Figure 7. Cross-section parallel to the A-B profile along Nodal Plane 1 (NP1) strike (274 degrees). The central negative $\Delta\boldsymbol{\sigma_c}$ zone (blue) corresponds to the coseismic slip area, flanked by positive $\Delta\boldsymbol{\sigma_c}$ lobes at both rupture terminations.

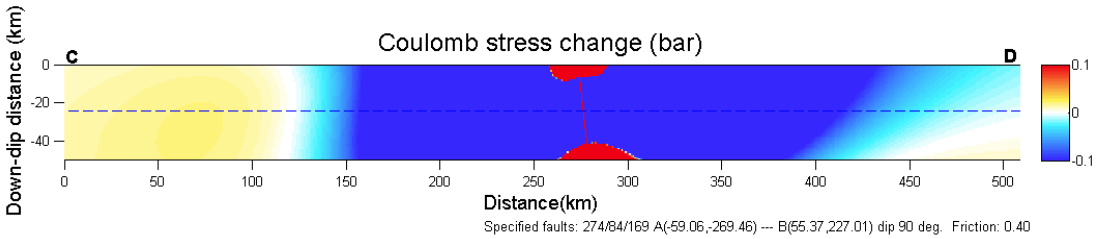

Figure 8. Cross-section perpendicular to the C-D profile, normal to the NP1 strike. The near-vertical stress transition boundary confirms rupture on a steeply dipping fault plane consistent with Nodal Plane 1 (NP1) (dip 84°).

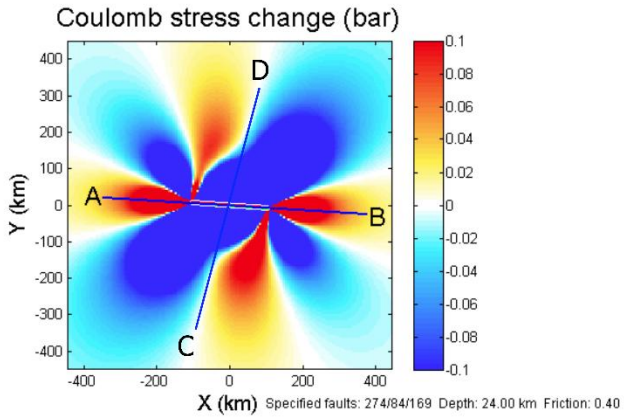

Figure 9 Map view showing the location of cross-section lines A-B and C-D

The cross-sectional analyses in Figures 7 and 8 provide depth-resolved confirmation of the Nodal Plane 1 rupture architecture. In the strike-parallel A-B section (Figure 7), the central negative $\Delta\sigma_c$ zone coincides precisely with the maximum coseismic slip area from the finite fault model, with symmetrical positive lobes at both rupture ends confirming bilateral propagation [31]. The strike-perpendicular C-D section (Figure 8) reveals a near-vertical stress boundary consistent with the steep dip of Nodal Plane 1 (84°), while localized positive $\Delta\sigma_c$ concentrations at the fault tips represent classic end-zone loading that promotes future rupture nucleation beyond the mainshock extent. The internal consistency between the finite fault slip distribution (Figure 3), the map-view $\Delta\sigma_c$ pattern (Figure 5), and the cross-sectional stress architecture (Figures 7 and 8) confirms that all results converge on Nodal Plane 1 as the true rupture plane. These findings are consistent with the physical expectation that only the true fault plane produces an on-fault stress release pattern with off-fault loading at the rupture terminations [32].

The positive Δσc zones identified in this study delineate areas of elevated seismic hazard in the southwestern Sumatran region. The loading zones at the Nodal Plane 1 rupture tips (Figures 5 and 7) indicate increased failure potential along northwest-southeast trending active structures, while the positive $\Delta\sigma_c$ on Nodal Plane 2 (NP2) highlights elevated risk on conjugate north-south trending fossil fracture zones [22]. These findings are consistent with Guo et al. (2021), who showed that post-earthquake seismicity in the Wharton Basin is concentrated in areas of positive Coulomb stress loading, confirming the predictive value of the $\Delta\sigma_c$ method for identifying future seismicity zones [6]. The results underscore the need to incorporate conjugate fault interactions and dynamic triggering mechanisms into seismic hazard models for the southern Wharton Basin, where simplified static stress models may systematically underestimate aftershock potential in high stress-drop intraplate environments [30].

4. Conclusion

This study applied the Coulomb stress change ($\Delta\sigma_c$) method to analyze the source mechanism and stress redistribution of the 2016 M_w 7.8 Southwest Sumatra earthquake. Three convergent lines of evidence confirm that Nodal Plane 1 (strike 274°, dip 84°, rake 169°) is the true fault plane controlling the earthquake source mechanism. The USGS finite fault model explicitly adopts the Nodal Plane 1 geometry with heterogeneous coseismic slip concentrated in a compact rupture of less than 70 km and a high stress drop of ~200 bar, characteristic of intraplate strike-slip ruptures on ancient oceanic crust. The cross-sectional $\Delta\sigma_c$ analysis reveals a classical on-fault stress release pattern, with negative $\Delta\sigma_c$at the slip center flanked by positive rupture-tip loading at both fault terminations. Orientation of Nodal Plane 1 is consistent with the dominant tectonic fabric and regional stress directions of the Wharton Basin, with a maximum $\Delta\sigma_c$ increase of 0.1 bar oriented west–east to northwest–southeast.

The spatial anomaly in which 71.43% of aftershocks fall within the negative $\Delta\sigma_c$ zones of Nodal Plane 1 is explained by three factors: the high coseismic stress drop of ~200 bar that creates an unusually broad stress shadow geometrically encompassing most proximal aftershock locations dynamic stress triggering by near-field seismic waves, which is known to produce aftershocks within static stress shadows; and uncertainties inherent in $\Delta\sigma_c$calculations particularly those arising from variations in receiver fault geometry, friction coefficient, and strike orientation of the receiver plane that may produce localized positive stress concentrations not fully resolved by the simplified elastic half-space model. Nodal Plane 2 functions as a receiver fault, where higher spatial consistency between positive $\Delta\sigma_c$ zones and aftershock distribution reflects static stress transfer onto conjugate north–south trending fossil fracture zones rather than primary rupture along Nodal Plane 2. These findings advance understanding of intraplate fault reactivation mechanics and static stress transfer dynamics in the southern Wharton Basin, contributing to more reliable seismic hazard assessment for the southwestern Sumatran region.

References

[1] Toda, S., & Stein, R. S. (2022). Central shutdown and surrounding activation of aftershocks from megathrust earthquake stress transfer. *Nature Geoscience*, *15*(6), 494-500.

[2] Jacob, J., Dyment, J., & Yatheesh, V. (2014). Revisiting the structure, age, and evolution of the Wharton Basin to better understand subduction under Indonesia. *Journal of Geophysical Research: Solid Earth*, *119*(1), 169-190.

[3] Putra, A. F., & Chenrai, P. (2022). Relative tectonic activity assessment of the Northern Sumatran Fault using geomorphic indices. *Frontiers in Earth Science*, *10*, 969170.

[4] Yutsis, V. V., Levchenko, O. V., Tevelev, A. V., Marinova, Y. G., Veklich, I. A., & Del Razo Gonzalez, A. (2024). Atypical Linear Tectonic Block of the Intraplate Deformation Zone in the Central Indian Ocean Basin. *Journal of Marine Science and Engineering*, *12*(12), 2231.

[5] Chen, J., Guo, L., Yang, X., Zhang, J., Zhang, Z., Sun, M., & Lin, J. (2023). Large Active Faults and the Wharton Basin Intraplate Earthquakes in the Eastern Indian Ocean. *Journal of Ocean University of China*, *22*(6), 1563-1571.
[6] Guo, L., Lin, J., Zhang, F., & Zhou, Z. (2021). Transfer of stress from the 2004 Mw9. 2 Sumatra subduction earthquake promoted widespread seismicity and large strike-slip events in the Wharton basin. *Terra Nova*, *33*(1), 74-85.
[7] "USGS Earthquake Hazards Program." Accessed: Jun. 12, 2026. [Online]. Available: https://earthquake.usgs.gov/
[8] Dahm, T., & Hainzl, S. (2022). A Coulomb stress response model for time-dependent earthquake forecasts. *Journal of Geophysical Research: Solid Earth*, *127*(9), e2022JB024443.
[9] Hardebeck, J., & Harris, R. (2025). Aftershocks in Stress Shadows are Inconsistent with Modeled Static Coulomb Stress Changes. *Seismica*, *4*(2).
[10] Sukrungsri, S., Khamsiri, S., & Pailoplee, S. (2024). Investigation of co-seismic stress and aftershock distribution along the Sumatra–Andaman subduction zone. *Geoscience Letters*, *11*(1), 48.
[11] Roodhiyah, L. Y., Nurhasan, Tiffany, Pratomo, P. M., Susilawati, A., Supriyadi, ... & Srigutomo, W. (2024). Interpretation of a 3D Magnetotellurics Model of the Aceh and Seulimeum Segments of the Sumatran Fault Zone. *Applied Sciences*, *14*(23), 11335.
[12] Triyoso, W., Kongko, W., Prasetya, G. S., & Sarsito, D. A. (2023). Spatial correlation of the maximum shear strain loading rate and the correlation dimension along the Sumatra subduction margin for potential earthquake and tsunami hazard study and analysis. *All Earth*, *35*(1), 287-301.
[13] Peng, Z., Lei, X., Wang, Q. Y., Wang, D., Mach, P., Yao, D., ... & Campillo, M. (2025). The evolution process between the earthquake swarm beneath the Noto Peninsula, Central Japan and the 2024 M 7.6 Noto Hanto earthquake sequence. *Earthquake Research Advances*, *5*(1), 100332.
[14] Hu, Y., Li, Z., Liu, R., & Wang, Z. (2023). Focal mechanism of Luding M 6.8 earthquake, September 2022 and analysis of the loading role of the tectonic stress on the seismogenic fault. *Earthquake Research Advances*, *3*(3), 100216.
[15] Zhou, M., Jin, Z., Wan, Y., & Guan, Z. (2026). Regional coulomb stress changes and stress triggering mechanisms of the noto M W7. 5 earthquake. *Journal of Seismology*, *30*(2), 24.
[16] Ekström, G., Nettles, M., & Dziewoński, A. M. (2012). The global CMT project 2004–2010: Centroid-moment tensors for 13,017 earthquakes. *Physics of the Earth and Planetary Interiors*, *200*, 1-9.
[17] Yun, J., Gabriel, A. A., May, D. A., & Fialko, Y. (2025). Controls of dynamic and static stress changes and aseismic slip on delayed earthquake triggering: Application to the 2019 Ridgecrest earthquake sequence. *Journal of Geophysical Research: Solid Earth*, *130*(12), e2025JB031271.
[18] Bonatis, P., Karakostas, V. G., Papadimitriou, E. E., & Kaviris, G. (2022). Investigation of the factors controlling the duration and productivity of aftershocks following strong earthquakes in Greece. *Geosciences*, *12*(9), 328.
[19] Kato, A., & Ben-Zion, Y. (2021). The generation of large earthquakes. *Nature Reviews Earth & Environment*, *2*(1), 26-39.
[20] Paul, H., Ravi Kumar, M., & Kumar, S. (2021). Evidence for reactivation of new faults and seismicity migration away from the causative fault of the 2001 MW 7.7 Bhuj earthquake, western India. *Geophysical Journal International*, *226*(3), 1800-1813.
[21] Fan, X., Zhang, G., & Shan, X. (2026). Static Stress Transfer and Fault Interaction Within the 2008–2020 Yutian Earthquake Sequence Constrained by InSAR-Derived Slip Models. *Remote Sensing*, *18*(2), 288.

[22] Sgambato, C., Faure Walker, J. P., Roberts, G. P., Mildon, Z. K., & Meschis, M. (2023). Influence of fault system geometry and slip rates on the relative role of coseismic and interseismic stresses on earthquake triggering and recurrence variability. *Journal of Geophysical Research: Solid Earth*, *128*(11), e2023JB026496.

[23] Chang, C. (2024). Identifying subsurface fault planes via a stress inversion of earthquake focal mechanisms. *Geophysical Journal International*, *236*(2), 1106-1124.

[24] Singh, S. C., Hananto, N., Qin, Y., Leclerc, F., Avianto, P., Tapponnier, P. E., ... & Barbot, S. (2017). The discovery of a conjugate system of faults in the Wharton Basin intraplate deformation zone. *Science Advances*, *3*(1), e1601689.

[25] Gunawan, E., Kongko, W., Kholil, M., Widyantoro, B. T., Widiyantoro, S., Supendi, P., ... & Gusman, A. R. (2022). The 2019 Mw 7.0 Banten, Indonesia, intraslab earthquake: investigation of the coseismic slip, tsunami modelling and Coulomb stress change. *Geoenvironmental Disasters*, *9*(1), 14.

[26] Lay, T., Ye, L., Ammon, C. J., Dunham, A., & Koper, K. D. (2016). The 2 March 2016 Wharton Basin Mw 7.8 earthquake: High stress drop north-south strike-slip rupture in the diffuse oceanic deformation zone between the Indian and Australian Plates. *Geophysical Research Letters*, *43*(15), 7937-7945.

[27] Hardebeck, J. L., & Harris, R. A. (2022). Earthquakes in the shadows: Why aftershocks occur at surprising locations. *The Seismic Record*, *2*(3), 207-216.

[28] Wulandari, R., Chan, C. H., & Wibowo, A. (2023). The 2022 Mw6. 2 Pasaman, Indonesia, earthquake sequence and its implication of seismic hazard in central-west Sumatra. *Geoscience Letters*, *10*(1), 25.

[29] Hardebeck, J. L. (2022). Physical properties of the crust influence aftershock locations. *Journal of Geophysical Research: Solid Earth*, *127*(10), e2022JB024727.

[30] Sgambato, C., Faure Walker, J. P., Mildon, Z. K., & Roberts, G. P. (2020). Stress loading history of earthquake faults influenced by fault/shear zone geometry and Coulomb pre-stress. *Scientific reports*, *10*(1), 12724.

[31] Ando, R., Fukushima, Y., Yoshida, K., & Imanishi, K. (2025). Nonplanar 3D fault geometry controls the spatiotemporal distributions of slip and uplift: evidence from the Mw 7.5 2024 Noto Peninsula, Japan, Earthquake. *Earth, Planets and Space*, *77*(1), 1-17.

[32] Ahadov, B., & Sh, J. (2023). The impact of Coulomb stress changes of the 2018 Mw 7.5 Palu earthquake, Indonesia. *ANAS Transactions, Earth Sciences*, no. 2